Applied Catalysis B: Environmental 84 (2008) 490–496

Contents lists available at ScienceDirect

Applied Catalysis B: Environmental

journal homepage: www.elsevier.com/locate/apcatb

The influence of precursors on Rh/SBA-15 catalysts for N_2O decomposition

Junming Du, Weiwei Kuang, Hualong Xu, Wei Shen *, Dongyuan Zhao *

Department of Chemistry and Shanghai Key Laboratory of Molecular and Innovative Materials, Fudan University, Shanghai 200433, People's Republic of China

ARTICLE INFO

Article history:
Received 15 January 2008
Received in revised form 8 May 2008
Accepted 9 May 2008
Available online 21 May 2008

Keywords:
N_2O decomposition
Rh/SBA-15
Precursors
Dispersion

ABSTRACT

Series of Rh/SBA-15 catalysts were prepared by impregnation and grafting method applying different Rh precursors. The catalytic behaviors of N_2O decomposition over these catalysts were tested in an automated eight flow reactor system. The catalysts were characterized by X-ray fluorescence spectroscopy (XRF), X-ray diffraction (XRD), N_2 adsorption/desorption, transmission electron microscopy (TEM) and X-ray photoelectron spectroscopy (XPS) techniques. The results showed that the dispersion of Rh species on the catalysts is closely related to the molecular size and the hydrophobic property of the precursors comparing to the hydrophilic support, better dispersion results were found in catalysts by impregnation of smaller precursors, while by grafting better dispersion resulted from big precursor. On the other hand, the activities of the catalysts match well with the Rh dispersion status. Rh/SBA-15-CDCR starting from $[(CO)_2RhCl]_2$ showed good dispersion and gave the best N_2O decomposition activity.

1. Introduction

Nitrous oxide (N_2O), is a greenhouse gas, which also contributes to the depleting of the ozone layer [1,2]. It has aroused great concern that the concentration of N_2O in the atmosphere is increasing by 0.2–0.3% per year, mainly caused by anthropogenic activities such as energy production and chemical processes. Thus reduction of anthropogenic N_2O emissions is urgently required, and catalytic direct N_2O decomposition is considered the most effective and economic method to fulfill the target. Many catalysts have been studied for this method, among them, Rh containing catalysts, either metal, pure oxides or supported oxides, exhibit comparatively high activities in catalytic direct N_2O decomposition [1–6].

Kondratenko et al. showed that the catalytic activity of pure Rh in direct N_2O decomposition increases with time-on-stream. The increase is explained by the transformation of metallic Rh to Rh_2O_3, which appears to be responsible for the resulting stability and activity [7]. For supported catalysts, Haber et al. investigated Rh catalysts on alumina and revealed that the addition of alkali metals influences the dispersion of Rh hence increase the activity [2]. Suarez et al. [8] and Boissel et al. [6] studied Rh catalystes over monolithic supports, Oi et al. examined the N_2O decomposition activities of Rh/ZnO, Rh/CeO_2, Rh/ZSM-5, ZnAlRh-hydrotalcite like compounds in his study [5,9], and Imamura et al. reported decomposition of N_2O on Rh/Pr/Ce and Rh/Zr/Ce composite oxides [10–13]. Yuzaki et al. gave the results of catalytic decomposition of N_2O over Rh catalysts supported on various supports (USY, NaY, Al_2O_3, ZrO_2, FSM-16, CeO_2, La_2O_3), the activities of Rh/Al_2O_3 and Rh/USY catalysts were comparable to or higher than the other catalysts due to the high Rh dispersion and also to the preparation variables such as the Rh precursors and the supports used [14,15]. In these literature, the activities of Rh are affected by the synergy effects with supports and greatly related to its dispersion. So far, the discussion about the effects of the precursors is restrained among $RhCl_3$ and $Rh(NO_3)_3$ as in Yuzaki et al.'s report [15], so it will be quite interesting to check the effect of other precursors on Rh dispersion and the N_2O decomposition activity.

In a previous study, mesoporous SBA-15 was chosen to be the support for Rh, in consideration of its high surface area, uniform pore size and good accessibility [3]. In the present paper, SBA-15 was still used as the supporting materials and several metallorganic Rh precursors were prepared and introduced into SBA-15 by impregnation and grafting method. The dispersion of Rh on the catalysts were examined and correlated to the size of precursors molecules. The activities of the catalysts were tested by an automated eight flow reactor system and proved to be closely related to the dispersion of Rh species.

2. Experimental

2.1. Catalysts preparation

SBA-15 was synthesized through a typical hydrothermal process as stated in reference using triblock copolymer

* Corresponding authors.
E-mail address: wshen@fudan.edu.cn (W. Shen).

0926-3373/$ – see front matter © 2008 Elsevier B.V. All rights reserved.
doi:10.1016/j.apcatb.2008.05.004

$EO_{20}PO_{70}EO_{20}$ (Pluronic P123) as organic template [16]. The calcined SBA-15 was used as carrier of the catalysts.

Several Rh compounds were synthesized starting from $RhCl_3{\cdot}3H_2O$ (Aldrich, abbreviated as RC) according to the literature and used as precursors to introduce Rh species into SBA-15. $ClRh(PPh_3)_3$ (chloro tristriphenylphosphine rhodium, abbreviated as CTPR) was prepared by mixing a solution of $RhCl_3{\cdot}3H_2O$ in ethanol with another solution of triphenylphosphine in ethanol under nitrogen [17]. $[(CO)_2RhCl]_2$ (chloro dicarbonyl rhodium dimmer, abbreviated as CDCR) was prepared by bubbling CO through a solution of $RhCl_3{\cdot}3H_2O$ in methanol for 20 h [18]. Then $[(CO)_2RhCl]_2$ was used to react with $BaCO_3$ and acetylacetone in petroleum ether under nitrogen to produce $(acac)Rh(CO)_2$ (acetylacetone dicarbonyl rhodium, abbreviated as ADCR). Finally $(acac)Rh(CO)PPh_3$ (acetylacetone carbonyl triphenylphosphine rhodium, abbreviated as ACTPR) was obtained from the reaction of $[Rh(acac)(CO)_2]$ with an equimolar amount of triphenylphosphine in hexane [19]. These precursors were then introduced into SBA-15 by impregnation method. SBA-15 used for support was preheated at 353 K for 1 h and then added the solution of the precursor. After that the mixture was dried at 353 K under N_2 flow and then calcined at 823 K for 3 h. The catalysts are denoted as Rh/SBA-15-x, where x stands for the abbreviation of its precursor. Grafting method was used as well to incorporate $ClRh(PPh_3)_3$ and $[(CO)_2RhCl]_2$ into SBA-15, the procedure was similar to the report of Calleja et al. [20]. The precursors were dissolved in CCl_4 and then SBA-15 was added to the solution. After 10 min stirring, 0.1 ml triethylamine was added to the suspension to promote surface silanols activation and the mixture was stirred for another 30 min. The solids were recovered by filtration and washed with ethanol, following by the same drying and calcinations as the impregnated catalysts. The catalysts prepared by grafting are denoted as Rh-SBA-15-x, x as precursor abbreviation.

2.2. Characterization

The catalysts were analyzed by XRF to determine the elemental compositions on a Bruker S4 Explorer using Rh as anode target material while the optimum test settings were predefined in SPECTRA^{PLUS}.

The nitrogen adsorption/desorption isotherms at 77 K were measured using a Micromeritics Tristar 3000 system. The pore structural data were analyzed by the BJH (Barrett–Joyner–Halenda) method using the Halsey equation for multilayer thickness. The pore size distribution curve came from the analysis of the adsorption branch of the isotherm.

XRD patterns were recorded with a Bruker D4 powder X-ray diffractometer, which employed Ni-filtered Cu Kα radiation and was operated at 40 kV and 40 mA. The scanning range of small-angle pattern was from $2\theta = 0.5$ to 5°, step interval 0.01°, while the range of wide-angle from $2\theta = 5$ to 60°, step interval 0.02°.

XPS measurements were performed in a Shimadzu Axis Ultra DLD system using a Al Kα (1486.6 eV) X-ray energy source. Characteristic photoemission peaks of Rh 3d were recorded with an energy resolution of 0.1 eV. Before XPS data analysis, the contribution of Al Kα3,4 satellite lines was eliminated and spectra were subjected to a Shirley-type background subtraction. Binding energies were calibrated using the carbon peak centered at 284.6 eV.

The prepared samples were also observed by TEM (JEOL JEM2011). The samples were supported on carbon-coated copper grids for the experiment.

2.3. Activity test

The catalytic decomposition of N_2O was carried out in an automated eight flow reactor system MTRS-1, designed by Fudan University and constructed by DADI. The catalysts granules with the particle size between 40 and 60 mesh were packed in the isothermal part of the quartz tubular reactor and SiO_2 was packed at both top and bottom of the catalyst bed. The catalysts were pretreated in a He flow at 673 K for 1 h. Then, the temperature was lowered to 573 K in He flow before the reaction started. The pressure was set to 0.3 MPa and the concentration of N_2O in He was 2600 ppm with the total GHSV at 19,000 h^{-1}. These conditions were set similar to the tail gas of nitric acid plant [1]. The reaction temperature was started at 573 K and raised at steps of 50–773 K. At each temperature the reactions were stabilized for 30 min before analysis started. After the performance was measured at 773 K, the temperature was lowered at steps of 100 K back to 573 K and the performance was measured similarly as during the heating. The gas was automatically sampled and analyzed by Finnigan TraceGC Ultra equipped with a thermal conductivity detector (TCD), using a Poraplot Q column (10 m).

3. Results and discussions

3.1. Catalysts characterization

The compositions, surface areas, pore diameters and volumes of the catalysts measured by XRF and N_2 adsorption/desorption are shown in Table 1. Rh loadings of most catalysts agree with the nominal result, however, Rh-SBA-15-CTPR prepared by grafting method contains only 0.4% Rh. Comparing to Rh-SBA-15-CDCR prepared by the same method, its precursor $ClRh(PPh_3)_3$ is much bigger in molecular size than $[(CO)_2RhCl]_2$ and much more hydrophobic, thus the precursor may be more difficult to diffuse into the pores of SBA-15 and to graft on the hydrophilic siliceous wall of the support. So that $ClRh(PPh_3)_3$ is more likely to aggregate because of intermolecular force and leach out during further washing after grafting. The surface areas of all catalysts drop in comparison to that of original SBA-15 but still reach over 550 m^2/g.

Fig. 1 shows the N_2 adsorption/desorption isotherms of the catalysts, which are typical H1 type for mesostructures with uniform cylindrical channels. The pore distribution of these catalysts derived from adsorption branches by BJH model are

Table 1
Textural properties of catalysts and SBA-15

Catalysts	Precursor	Rh loading (wt%)	Surface area ($m^2\ g^{-1}$)	Pore diameter (nm)	Pore volume ($cm^3\ g^{-1}$)
Rh/SBA-15-RC	$RhCl_3$	0.93	579	6.1	0.90
Rh/SBA-15-CTPR	$ClRh(PPh_3)_3$	0.96	573	6.3	0.94
Rh/SBA-15-CDCR	$[(CO)_2RhCl]_2$	1.03	589	6.3	0.93
Rh/SBA-15-ADCR	$(acac)Rh(CO)_2$	1.02	593	6.4	0.95
Rh/SBA-15-ACTPR	$(acac)Rh(CO)PPh_3$	0.98	575	6.8	0.99
Rh-SBA-15-CTPR	$ClRh(PPh_3)_3$	0.40	552	7.1	1.01
Rh-SBA-15-CDCR	$[(CO)_2RhCl]_2$	0.99	545	7.4	1.03
SBA-15	–	–	845	7.2	1.39

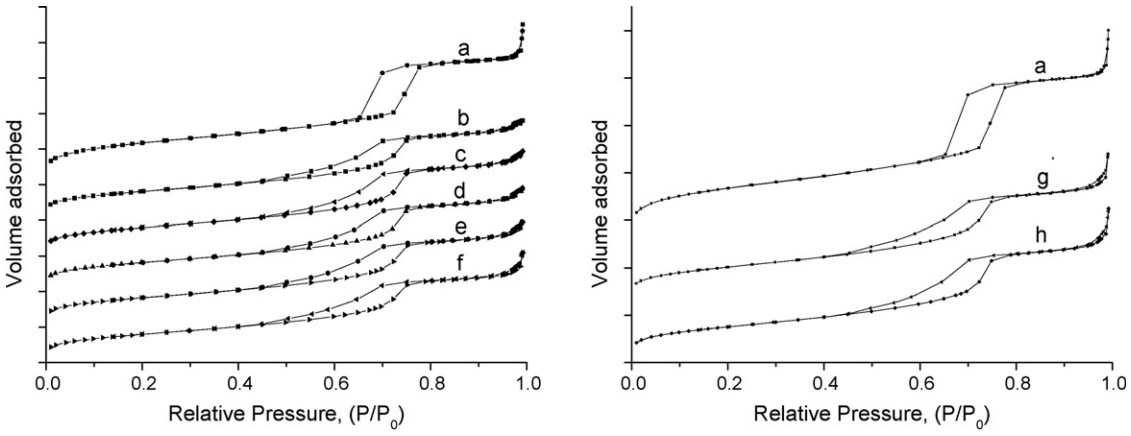

Fig. 1. N_2 adsorption/desorption isotherms of catalysts: (a) SBA-15, (b) Rh/SBA-15-RC, (c) Rh/SBA-15-CTPR, (d) Rh/SBA-15-CDCR, (e) Rh/SBA-15-ADCR, (f) Rh/SBA-15-ACTPR, (g) Rh-SBA-15-CTPR, (h) Rh-SBA-15-CDCR.

given in Fig. 2. All the catalysts show a widened range of pore diameter shifted to small pore diameter after the loading of Rh species.

XRD patterns of the catalysts prepared by impregnation are shown in Fig. 3. In the small-angle range, all samples show the typical pattern of hexagonal structure with a very strong diffraction peak near 1° attributed to (1 0 0) and two weaker peaks indexed to (1 1 0) and (2 0 0) of SBA-15 as reported [16]. XRD results indicate that the catalysts kept the ordered structure of SBA-15. On the other hand, no obvious diffraction peaks are found in the wide-angle area except the broad one for amorphous SiO_2, probably due to the small amount of Rh and relatively high surface area of SBA-15. Fig. 4 shows the XRD patterns of the catalysts prepared by grafting, which are similar to those of impregnated ones.

Fig. 5 shows the XPS spectra of all the catalysts samples with the fitting results presented in Table 2. Rh $3d_{5/2}$ peak was observed at

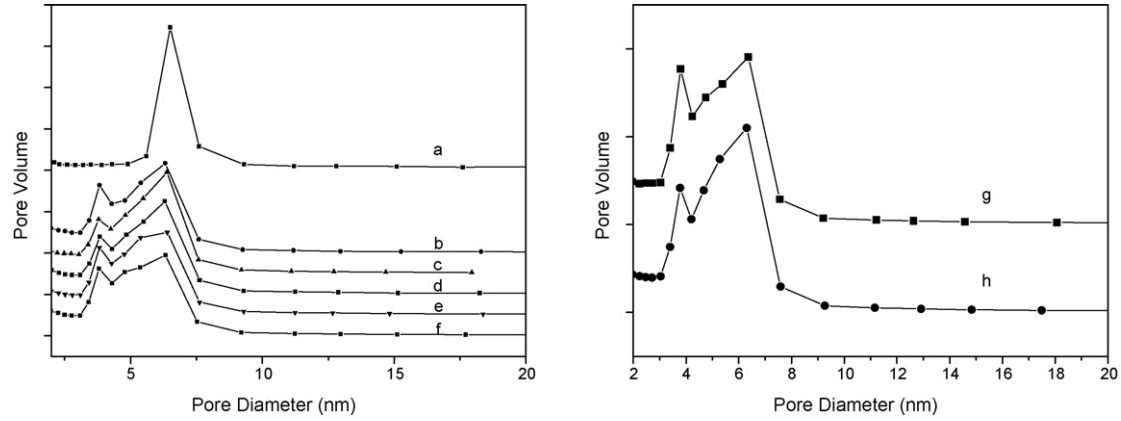

Fig. 2. Pore diameter distributions of catalysts: (a) SBA-15, (b) Rh/SBA-15-RC, (c) Rh/SBA-15-CTPR, (d) Rh/SBA-15-CDCR, (e) Rh/SBA-15-ADCR, (f) Rh/SBA-15-ACTPR, (g) Rh-SBA-15-CTPR, (h) Rh-SBA-15-CDCR.

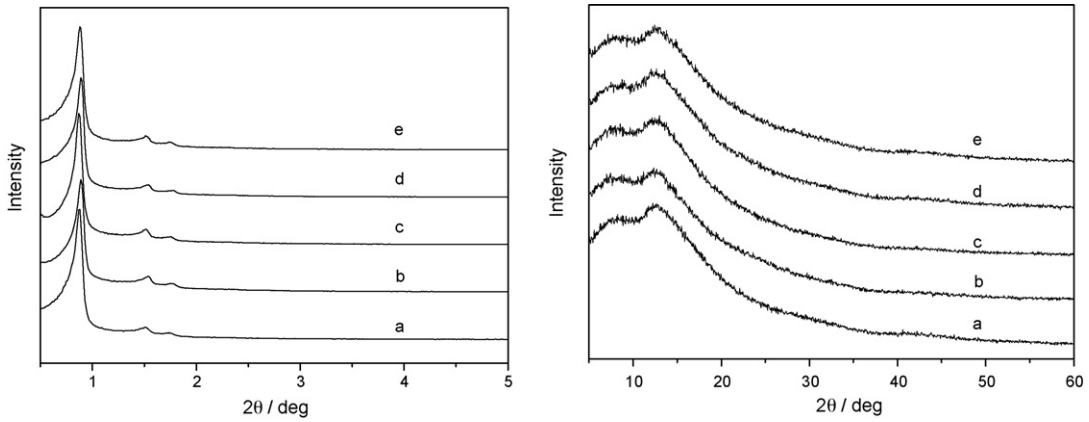

Fig. 3. XRD patterns of Rh/SBA-15: (a) Rh/SBA-15-RC, (b) Rh/SBA-15-CTPR, (c) Rh/SBA-15-CDCR, (d) Rh/SBA-15-ADCR, (e) Rh/SBA-15-ACTPR.

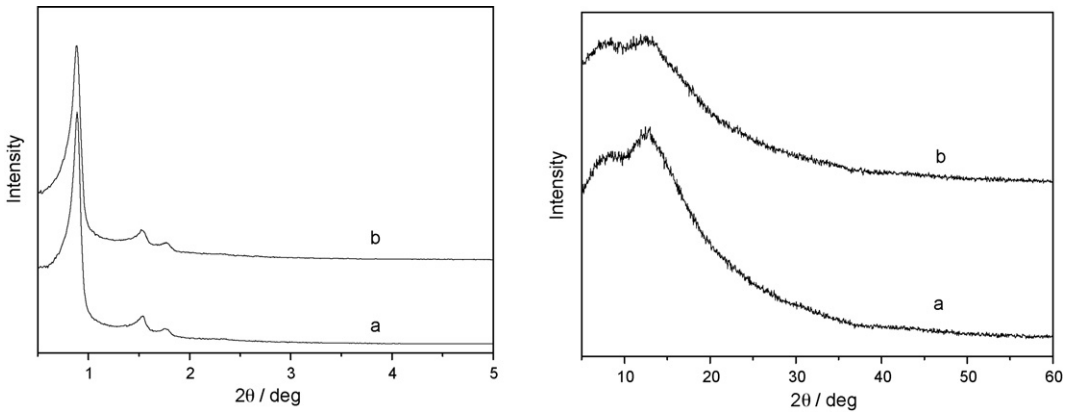

Fig. 4. XRD patterns of Rh-SBA-15: (a) Rh-SBA-15-CTPR, (b) Rh-SBA-15-CDCR.

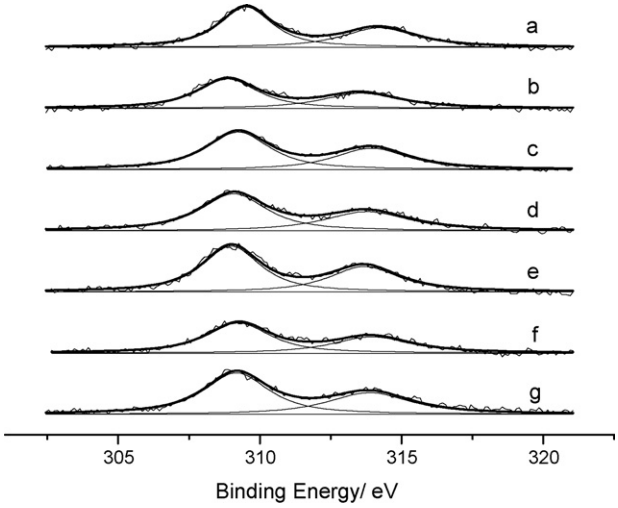

Fig. 5. XPS results: (a) Rh/SBA-15-RC, (b) Rh/SBA-15-CTPR, (c) Rh/SBA-15-CDCR, (d) Rh/SBA-15-ADCR, (e) Rh/SBA-15-ACTPR, (f) Rh-SBA-15-CTPR, (g) Rh-SBA-15-CDCR.

around 309 eV with its accompanying $3d_{3/2}$ peak about 314 eV in all the spectra, which indicates that Rh is in the form of oxidized state Rh^{3+} [7,21,22]. Considering the oxidative environment in the activity tests, it can be deduced that it is Rh^{3+} played the role of active center rather than the metallic state in our experiments [5]. It is noticeable that in the spectrum of Rh/SBA-15-RC, the peaks shift to higher binding energy possibly due to residue of Cl, as in XRF result, Rh/SBA-15-RC was the only sample containing Cl at about 0.4%.

It is also acknowledged that the XPS ratio, as shown by Formula (1), can indicate the dispersion of the active phase A at the surface of the support phase B in the case of heterogeneous catalysts. An increase of the phase A/phase B ratio is related to an increase of the spreading of phase A on the surface of phase B, vice versa [22,23]. In our case, the XPS ratios of Rh to Si were summarized in Table 2 as well, and the relative dispersion were calculated taking the Rh/SBA-15-CDCR as 100%, which gives out the highest ratio.

$$\text{XPS ratio} = \frac{\text{atomic concentration of the metal from the active phase (Rh) (\%)}}{\text{atomic concentration of the element of support (Si) (\%)}} \quad (1)$$

TEM images of the catalysts prepared by impregnation are displayed in Fig. 6, all with typical SBA-15 nanosized tunnels. Rh/SBA-15-RC (1a, 1b) and Rh/SBA-15-CDCR (3a, 3b) show the clearest mesostructures among others, with no large Rh particles presented in TEM images. Rh/SBA-15-ADCR (4a, 4b) seems to have some small Rh-species attached to the siliceous walls. However it is not so clear at the scale of our TEM results. But in the TEM image of Rh/SBA-15-CTPR (2a, 2b), it is very clear that the Rh was aggregated to small particles which almost blocked the tunnels. Aggregated Rh species can also be found in Rh/SBA-15-ACTPR (5a, 5b), but unlike Rh/SBA-15-CTPR, the particles are probably located on the outer surface of SBA-15. The dispersion status is related to the precursor molecules characteristics. The precursors of Rh/SBA-15-RC, Rh/SBA-15-CDCR and Rh/SBA-15-ADCR are $RhCl_3$, $[(CO)_2RhCl]_2$ and $(acac)Rh(CO)_2$, respectively, quite small and hydrophilic molecules comparing to those precursors with triphenylphosphine. So these precursors can be easily diffused to the SBA-15 tunnels around 7 nm and dispersed over the walls of the supporting materials. The precursors $ClRh(PPh_3)_3$ and $(acac)Rh(CO)PPh_3$ for Rh/SBA-15-CTPR and Rh/SBA-15-ACTPR are not only big in molecular size, but also more hydrophobic. Therefore during the impregnation process, they may be more likely to congregate into big particles by the

Table 2
Peak fitting results and dispersion estimation from XPS

	Binding energy (eV)			XPS ratio $Rh_{3d5/2}/Si_{2p}$ (10^{-3})	Relative dispersion (%)
	$Rh_{3d5/2}$	$Rh_{3d3/2}$	Si_{2p}		
Rh/SBA-15-RC	309.6	314.3	103.6	4.67	66.6
Rh/SBA-15-CTPR	309.0	313.6	103.6	3.63	50.2
Rh/SBA-15-CDCR	309.2	313.9	103.6	7.75	100.0
Rh/SBA-15-ADCR	309.1	313.8	103.7	5.75	74.8
Rh/SBA-15-ACTPR	309.0	313.7	103.6	3.87	52.4
Rh-SBA-15-CTPR	309.3	313.9	103.5	2.31	76.8
Rh-SBA-15-CDCR	309.2	313.9	103.6	4.17	56.0
Ref. [21]	309.2	–	–	–	–

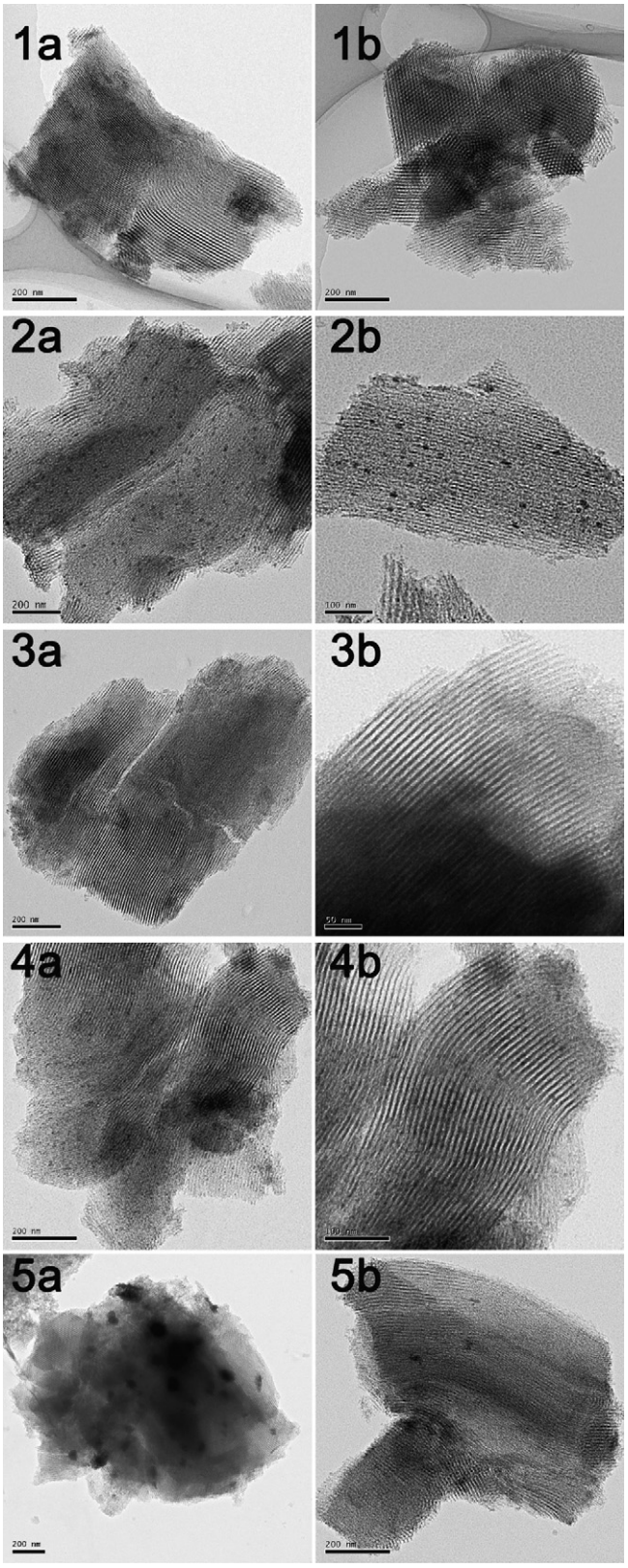

Fig. 6. TEM image of catalysts prepared by impregnation: (1a, 1b) Rh/SBA-15-RC, (2a, 2b) Rh/SBA-15-CTPR, (3a, 3b) Rh/SBA-15-CDCR, (4a, 4b) Rh/SBA-15-ADCR, (5a, 5b) Rh/SBA-15-ACTPR.

intermolecular forces of phenyls than evenly disperse on the mesoporous SBA-15 walls with quite much silanols [24]. It have been reported that the hydrophobic or hydrophilic nature of catalyst support materials may influence the reaction behavior [25], and in our case, the hydrophobic and hydrophilic nature of the catalysts precursors affects the active component dispersion over the support materials.

On the other hand, it is quite interesting to find in Fig. 7 that both catalysts prepared by grafting method show Rh particles inside SBA-15 tunnels, and the larger particle size is found in Rh-SBA-15-CDCR (2a, 2b), though its precursor $[(CO)_2RhCl]_2$ is much smaller than the $ClRh(PPh_3)_3$ for Rh-SBA-15-CTPR. In the TEM image, it is seen that the Rh particles of Rh-SBA-15-CDCR cover the range about 4–5 tunnels. It has been stated [26] that one distinguish property of SBA-15 is the micromesoporous ranged windows on its siliceous walls, and several groups have taken advantage of the characteristic to prepare well ordered 2D nanoarrays of carbon and metallic compounds by filling up the nanochannels by suitable materials [27]. In our case, it can be deduced that the small molecules of $[(CO)_2RhCl]_2$ were dispersed into the windows in liquid environment and connected Rh species across the channels to produce large particles. On the contrary, $ClRh(PPh_3)_3$ with comparative size to the microporous windows and hydrophobic groups can hardly enter the windows so that the Rh particles in Rh-SBA-15-CTPR were limited in single tunnel, quite similar to Rh/SBA-15-CTPR.

Comparing the TEM images with the dispersion data in Table 2, it is quite clear that by impregnation, the two catalysts from triphenylphosphine compounds show worse dispersion than the others, and by grafting, though the Rh dispersion of Rh-SBA-15-CTPR is higher, it suffers a great loss in Rh loading.

3.2. N_2O decomposition activities

The N_2O decomposition activities of the catalysts under different temperatures are shown in Fig. 8. The parent SBA-15 shows no activity, which also implies that no thermal decomposition of N_2O occurs in the temperature range of our experiment.

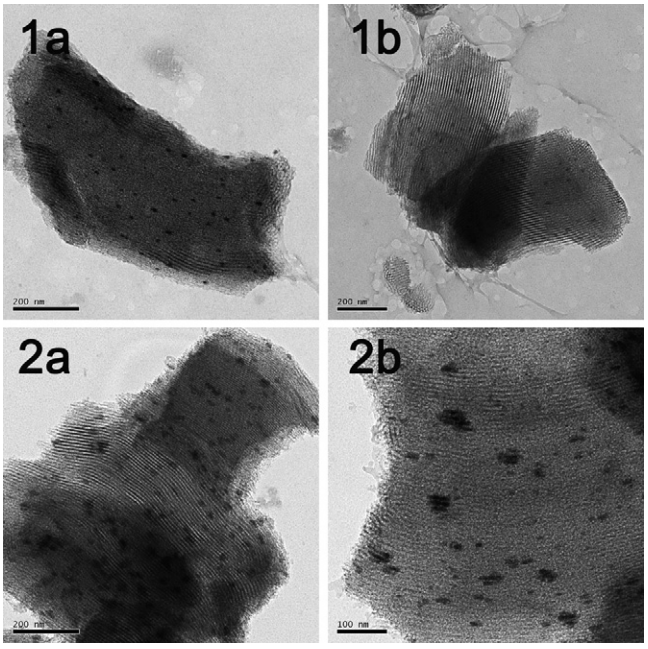

Fig. 7. TEM image of catalysts prepared by grafting: (1a, 1b) Rh-SBA-15-CTPR, (2a, 2b) Rh-SBA-15-CDCR.

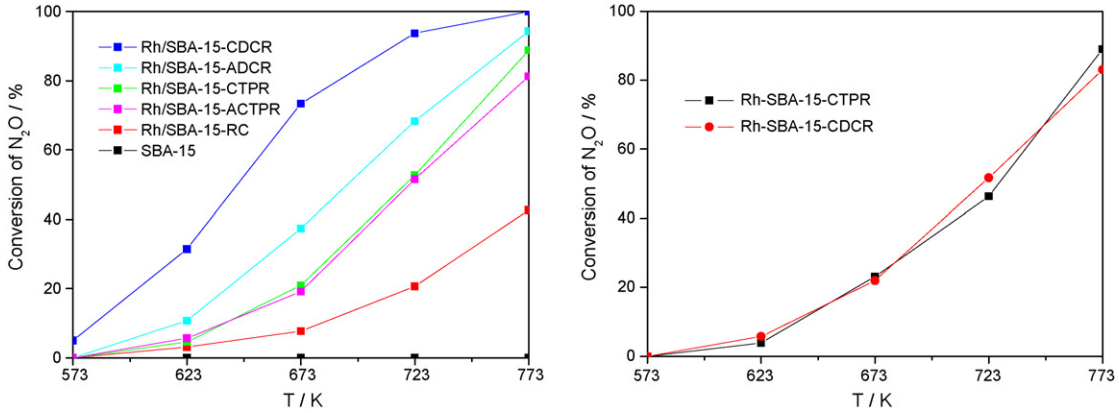

Fig. 8. N_2O decomposition over different catalysts.

Table 3
Dispersion and N_2O decomposition activities of the catalysts

	Rh precursor size (nm)	Rh loading (wt%)	Relative dispersion (%)	T_{50} (K)[a]	Relative TOF (10^{-3} s^{-1})[b]
Rh/SBA-15-RC	0.2	0.93	66.6	N/A	1.6
Rh/SBA-15-CTPR	1.0	0.96	50.2	718	4.1
Rh/SBA-15-CDCR	0.6	1.03	100.0	645	13.3
Rh/SBA-15-ADCR	0.5	1.02	74.8	693	6.8
Rh/SBA-15-ACTPR	0.8	0.98	52.4	720	3.6
Rh-SBA-15-CTPR	1.0	0.4	76.8	727	10.3
Rh-SBA-15-CDCR	0.6	0.99	56.0	720	4.3

[a] Estimated data from Fig. 8.
[b] TOF value at 673 K.

Among the catalysts prepared by impregnation, Rh/SBA-15-CDCR gives out the best performance, the activity rises rapidly at relatively low temperature and reaches full N_2O conversion at 773 K. The activity of Rh/SBA-15-ADCR is lower than Rh/SBA-15-CDCR, but slightly higher than those of Rh/SBA-15-CTPR and Rh/SBA-15-ACTPR. The trend in the activities change corresponds well with the dispersion status of Rh species on SBA-15 discussed earlier, that the better the dispersion is, the higher the activity. The only exception is Rh/SBA-15-RC, which shows no nanocrystals in the mesochannels of SBA-15 at all but turns out to have the worst activity, less than 50% N_2O conversion even at 773 K. The reason may be the excess residual Cl from the precursor $RhCl_3$, which could suppress the activity of N_2O decomposition as previously reported by Yuzaki et al. [15]. Taking the XPS results into consideration, the excessive positive charge of Rh species on Rh/SBA-15-RC might be the reason for the low N_2O decomposition activity.

The catalytic activities of Rh-SBA-15-CDCR and Rh-SBA-15-CTPR prepared by grafting are pretty similar. However, taking the low Rh loading on Rh-SBA-15-CTPR into consideration, it still leads to the deduction that the higher activity will be achieved on better dispersed catalyst.

Another summary of the N_2O decomposition catalytic activity was made in Table 3 with T_{50} (at which 50% conversion is achieved) and TOF data. The lowest T_{50} and highest TOF are achieved on Rh/SBA-15-CDCR, which also holds the best dispersion. Those catalysts with similar relative dispersion around 50%, including Rh/SBA-15-CTPR, Rh/SBA-15-ACTPR and Rh-SBA-15-CDCR, give out the similar activity result. The T_{50} of N_2O over Rh-SBA-15-CTPR is almost the same as the three catalysts mentioned above, however, in term of TOF, it excels those catalysts with worse dispersion. The result of Rh/SBA-15-RC is quite exceptional as discussed above.

4. Conclusion

Series of Rh-containing metallorganic compounds were synthesized and introduced into SBA-15 by impregnation or grafting method. The dispersion of Rh species on the catalysts prepared by impregnation is closely related to the nature of the precursors. The catalysts using carbonyl compounds as precursors apparently excel in Rh dispersion than those from triphenylphosphine precursors because of the hydrophilicity and the small size. While on catalysts prepared by grafting method, due to the increase in mobility, the small precursor $[(CO)_2RhCl]_2$ was easily diffused into the micromesoporous windows on SBA-15 walls and connect Rh species in adjacent channels, as a result, Rh dispersion was worse than that using $ClRh(PPh_3)_3$.

The activity tests of N_2O decomposition on these catalysts were carried out in an automated eight flow reactor system. The activities of the catalysts correspond well with the Rh dispersion status, both in impregnated and grafted catalysts, except for Rh/SBA-15-RC, which is the most inactive catalyst, possibly due to higher binding energy of Rh related to residue of Cl.

Acknowledgements

We gratefully thank financial support from Shanghai Key Laboratory of Molecular and Innovative Materials and the assistance of Prof. Zhen Pang in the synthesis of metallorganic compounds.

References

[1] F. Kapteijn, J. Rodriguez Mirasol, J.A. Moulijn, Appl. Catal. B: Environ. 9 (1–4) (1996) 25.
[2] J. Haber, M. Nattich, T. Machej, Appl. Catal. B: Environ. 77 (3–4) (2008) 278.
[3] X. Xu, H. Xu, F. Kapteijn, J. Moulijn, Appl. Catal. B: Environ. 53 (4) (2004) 265.

[4] K. Doi, Y. Wu, R. Takeda, A. Matsunami, N. Arai, T. Tagawa, S. Goto, Appl. Catal. B: Environ. 35 (1) (2001) 43.
[5] J. Oi, A. Obuchi, G. Bamwenda, A. Ogata, H. Yagita, S. Kushiyama, K. Mizuno, Appl. Catal. B: Environ. 12 (4) (1997) 277.
[6] V. Boissel, S. Tahir, C.A. Koh, Appl. Catal. B: Environ. 64 (3–4) (2006) 234.
[7] E. Kondratenko, R. Kraehnert, J. Radnik, M. Baerns, J. Perez-Ramirez, Appl. Catal. A: Gen. 298 (2006) 73.
[8] S. Suarez, M. Yates, A.L. Petre, J.A. Martin, P. Avila, J. Blanco, Appl. Catal. B: Environ. 64 (3–4) (2006) 302.
[9] J. Oi, A. Obuchi, A. Ogata, G. Bamwenda, R. Tanaka, T. Hibino, S. Kushiyama, Appl. Catal. B: Environ. 13 (3–4) (1997) 197.
[10] S. Imamura, J. Tadani, Y. Saito, Y. Okamoto, H. Jindai, C. Kaito, Appl. Catal. A: Gen. 201 (1) (2000) 121.
[11] S. Imamura, R. Hamada, Y. Saito, K. Hashimoto, H. Jindai, J. Mol. Catal. A: Chem. 139 (1) (1999) 55.
[12] K. Hashimoto, N. Toukai, R. Hamada, S. Imamura, Catal. Lett. 50 (3–4) (1998) 193.
[13] S. Imamura, T. Kitao, H. Kanai, S. Shono, K. Utani, H. Jindai, React. Kinet. Catal. Lett. 61 (1) (1997) 201.
[14] K. Yuzaki, T. Yarimizu, S. Ito, K. Kunimori, Catal. Lett. 47 (3–4) (1997) 173.
[15] K. Yuzaki, T. Yarimizu, K. Aoyagi, S. Ito, K. Kunimori, Catal. Today 45 (1–4) (1998) 129.
[16] D.Y. Zhao, J.L. Feng, Q.S. Huo, N. Melosh, G.H. Fredrickson, B.F. Chmelka, G.D. Stucky, Science 279 (5350) (1998) 548.
[17] P.G. Gassman, D.W. Macomber, S.M. Willging, J. Am. Chem. Soc. 107 (8) (1985) 2380.
[18] F. Malbosc, V. Chauby, C. Serra-Le Berre, M. Etienne, J.C. Daran, P. Kalck, Eur. J. Inorg. Chem. (10) (2001) 2689.
[19] A.M. Trzeciak, B. Borak, Z. Ciunik, J.J. Ziolkowski, M.F.C.G. da Silva, A.J.L. Pombeiro, Eur. J. Inorg. Chem. (7) (2004) 1411.
[20] G. Calleja, R. van Grieken, R. Garcia, J.A. Melero, J. Iglesias, J. Mol. Catal. A: Chem. 182 (1) (2002) 215.
[21] C. Force, E. Roman, J.M. Guil, J. Sanz, Langmuir 23 (8) (2007) 4569.
[22] P.S. Lambrou, P.G. Savva, J.L.G. Fierro, A.A. Efstathiou, Appl. Catal. B: Environ. 76 (3–4) (2007) 375.
[23] F. Bertinchamps, C. Gregoire, E.M. Gaigneaux, Appl. Catal. B: Environ. 66 (1–2) (2006) 1.
[24] J. Pires, M. Pinto, J. Estella, J.C. Echeverria, J. Colloid Interface Sci. 317 (1) (2008) 206.
[25] F. Omota, A.C. Dimian, A. Bliek, Appl. Catal. A: Gen. 294 (2) (2005) 121.
[26] R. Ryoo, C.H. Ko, M. Kruk, V. Antochshuk, M. Jaroniec, J. Phys. Chem. B 104 (48) (2000) 11465.
[27] B.Z. Tian, X.Y. Liu, H.F. Yang, S.H. Xie, C.Z. Yu, B. Tu, D.Y. Zhao, Adv. Mater. 15 (16) (2003) 1370.